CALT-68-522
INTERNAL REPORT
Not for Distribution
FERMILAB-PUB-75-178-E

#268

The Ratio $\sigma(pp \to \pi^o X)/\sigma(\pi^+ p \to \pi^o X)$ at Large Momentum Transfer and Quark-Quark Scattering*

R. D. Field and D. J. Mellema

California Institute of Technology, Pasadena, California 91125

ABSTRACT

We present a phenomenological "first look" at new Fermilab inclusive data on large $p_\perp$ π^o production in pp and $\pi^+ p$ collisions at $\theta_{cm} \simeq 90^o$. Predictions are made using a simple model in which particles are produced at large transverse momentum by a single, hard, large-angle scattering between quarks ($q + q \to q + q$). In this model the ratio $R = \sigma(pp \to \pi^o X)/\sigma(\pi^+ p \to \pi^o X)$ is determined by the difference in the structure functions of the incident proton or pion. This interpretation is consistent with the new $\theta_{cm} = 90^o$ data and suggests the importance of measuring R at other θ_{cm} values.

*Work supported in part by the U. S. Energy Research and Development Administration under Contract No. AT(11-1)-68 for the San Francisco Operations Office.

I. Introduction.

One of the most exciting aspects of large transverse momentum hadron reactions is the possibility of probing the simplest constituent structure and the underlying dynamics of hadronic matter at short distances. In the case of deep inelastic lepton scattering, Bjorken scaling implies that a finite fraction of a nucleon's momentum is carried by point like constituents[1,2] (or quarks). Accordingly, in the case of hadronic collisions, one expects that particles can be produced at large transverse momentum by a single, hard, large-angle scattering involving these constituents[3]. On the other hand, the fact that large $p_\perp$ hadronic cross sections are large (do not fall like $\exp(-6p_\perp)$) does not in itself verify the constituent nature of hadrons. Other, more conventional (strictly hadronic) descriptions have been used to "explain" the observed production cross sections[4].

One important and exciting way to investigate the constituent (quark) nature of hadrons is to compare the large $p_\perp$ invariant cross sections for $pp \to \pi^o X$ and $\pi^+ p \to \pi^o X$. Constituent quark models predict definite differences in these processes due to the differing quark distributions within the proton and pion beam and/or due to differing sub-processes.

In this paper we discuss predictions for the ratio $R = \sigma(pp \to \pi^o X)/\sigma(\pi^+ p \to \pi^o X)$ based on simple constituent quark ideas. These predictions are compared with preliminary data from Fermilab Experiment #268, obtained at $\theta_{cm} = 90^o$ and $p_{lab} = 100$ and 200 GeV/c. Many of the points presented in this paper do not depend on the detailed mechanism assumed for the interactions between quarks but merely upon the hypothesis that it is the interaction between constituents that is responsible for large $p_\perp$ hadronic production. In addition we stress the importance of acquiring data at angles other than 90^o.

II. Formalism.

All of the constituent or "hard-scattering" models which have been proposed to describe the hadronic process $A + B \to C + X$ at large transverse momentum have the common underlying structure illustrated in Fig. 1. In the hard-scattering models the large transverse momentum reaction is assumed to occur as the result of a single large angle scattering $a + b \to c + d$ of constituents a and b, followed in general by the decay or fragmentation of c into the observed particle C [5]. Particular models differ in the choice of the basic interaction $d\hat{\sigma}/d\hat{t}\ (\hat{s},\hat{t};\ a + b \to c + d)$. For quark-quark scattering this interaction is of course $q + q \to q + q$, where q is a quark (Fig. 2) [2,6]. In the constituent interchange model[7] (CIM), the underlying large angle reaction involves quark-hadron scattering (e.g. $q + \pi \to q + \pi$). In the multiperipheral type models, the large angle process involves only hadrons (e.g. $\pi + \pi \to \pi + \pi$)[8].

The calculation of the cross-section corresponding to Fig. 1 has the following form:

$$E\, d\sigma/d^3p\ (s,t,u;\ A + B \to C + X) =$$

$$\int_{x_a^{min}}^{1} dx_a \int_{x_b^{min}}^{1} dx_b\ G_{A\to a}(x_a)\ G_{B\to b}(x_b)\ H_{c\to C}(x_c)\ \frac{1}{x_c}\left[\frac{1}{\pi}\frac{d\hat{\sigma}}{d\hat{t}}\ (\hat{s},\hat{t};\ a + b \to c + d)\right] \tag{2.1}$$

where

$$\hat{s} = x_a x_b s$$

$$\hat{t} = \frac{x_a}{x_c}\, t$$

$$\hat{u} = \frac{x_b}{x_c}\, u\ . \tag{2.2}$$

In addition, $\hat{s} + \hat{t} + \hat{u} = \sum m^2 \simeq 0$ implies

$$x_c = \frac{x_2}{x_b} + \frac{x_1}{x_a} \quad , \text{ with } x_2 = -\frac{t}{s},\ x_1 = -\frac{u}{s} .$$

Also note that $x_2 = \frac{1}{2} x_\perp \tan \frac{1}{2}\theta$ and $x_1 = \frac{1}{2} x_\perp \cot \frac{1}{2}\theta$, where θ is the center of mass scattering angle[9]. Here $G_{A\to a}(x_a)$ etc. is the probability for the constituent or fragment a to have fractional longitudinal momentum x_a in a frame where $|P_A| \to \infty$. For the case where a is a quark the Bjorken scaling function $\nu W_2(x)$ is

$$\nu W_2^A(x) = \sum_q e_q^2 \, x \, G_{A\to q}(x) \ , \tag{2.3}$$

where $x = -Q^2/2m\nu$.

(i) Power Counting.

Assuming that the differential cross section for $a + b \to c + d$ behaves like a power at large $\hat{s}$, $\hat{t}$; namely,

$$\frac{d\hat{\sigma}}{d\hat{t}}(\hat{s},\hat{t};\ a + b \to c + d) \sim \frac{1}{\hat{s}^N} f\left(\frac{\hat{t}}{\hat{s}}\right) \ , \tag{2.4}$$

then (2.1) yields a cross section of the asymptotic form

$$E\, d\sigma/d^3p\ (s,t,u;\ A + B \to C + X) \sim \boxed{\sum_{abc} \varepsilon^f \left(p_\perp^2 + M^2\right)^{-N} I(x_\perp, \theta_{cm}),} \tag{2.5}$$

where $\varepsilon = 1 - x_\perp$

and the "forbiddeness" f is given by

$$f = f_a + f_b + f_c + 2 \tag{2.6}$$

with

$$G_{A\to a}(x_a) \sim (1 - x_a)^{f_a}$$

$$G_{B\to b}(x_b) \sim (1 - x_b)^{f_b}$$

$$G_{c\to C}(x_c) \sim (1 - x_c)^{f_c} \quad . \tag{2.7}$$

Thus at fixed $x_\perp$ and θ_{cm} the $p_\perp$ dependence of the invariant cross section is governed by the power dependence (2.4) of $d\hat{\sigma}/d\hat{t}(a + b \to c + d)$, whereas at fixed $p_\perp$ and θ_{cm} the ϵ dependence is governed by the distribution functions (2.7).

Fixed: $x_\perp, \theta_{cm}$ (vary $p_\perp$) — See power dependence

Fixed: $p_\perp, \theta_{cm}$ (vary $x_\perp$) - See quark distribution functions

(ii) Quark-quark Scattering.

In the most naive case the differential cross section for quark-quark elastic scattering (Fig. 2b) is given by

$$\frac{d\hat{\sigma}}{d\hat{t}}(\hat{s},\hat{t};\ qq \to qq) = 2\pi\left(\frac{g^2}{4\pi}\right)^2 (\hat{s}^2 + \hat{u}^2)/(\hat{s}^2\hat{t}^2) \ , \tag{2.8}$$

where we have assumed the exchange of a single vector-gluon with coupling strength $g^2/4\pi$. This cross-section behaves like $1/\hat{s}^2$ for large $\hat{s},\hat{t}$, which results [(2.4) and (2.5)] in an invariant cross section which behaves like $1/p_\perp^4$ for fixed $x_\perp$ and θ_{cm}.

Existing data from both FNAL and ISR clearly rule out the presence of such a term as the dominant mechanism for large $p_\perp$ production[10]. We are thus left with the following alternatives.

1. We can abandon quark-quark scattering (arbitrarily ignore it) as the dominant mechanism and look for other basic interactions like $q\pi \to q\pi$ or $q(qq) \to \pi N^*$ which result in cross section behavior in more agreement with data[11], but which are not as esthetically pleasing.

2. We can take the viewpoint that quark-quark scattering is indeed the important mechanism for large $p_\perp$ hadronic scattering but that the

above calculations which led to $1/p_\perp^4$ behavior were simply too naive. Perhaps the fragmentation of a quark into a pion ("dressing the quark") is more complicated than the distribution $H_{q\to\pi^o}(x)$ indicates (it may contain non-scaling pieces[12]) or perhaps the basic quark-quark scattering $d\hat{\sigma}/d\hat{t}$ is not as simple as (2.8). The "effective" coupling constants $g^2/4\pi$ of the gluon may depend on the scattering variables $\hat{s}$ and/or $\hat{t}$ in some way[13].

In this paper we adopt the second viewpoint and "doctor up" the quark-quark interaction $d\hat{\sigma}/d\hat{t}$ $(\hat{s},\hat{t};\ q + q \to q + q)$ to yield the observed $1/p_\perp^{12}$ behavior seen at FNAL[14]. Many of our results will not depend greatly on the details of how one modifies the quark-quark interaction but instead depend on the more general hypothesis that quark-quark scattering is indeed the important mechanism. In particular the ratio R will now be simply a consequence of the difference in the structure functions for the pion and proton beam. In Sec. IV we discuss briefly the results of other approaches.

(iii) Quark Distributions $G_{p\to q}(x)$, $G_{\pi\to q}(x)$.

The quark distributions within a proton are fairly well known from the deep inelastic electron proton $(\nu W_2^p(x))$ and electron neutron $(\nu W_2^n(x))$ scattering structure functions. From (2.3) we have

$$\nu W_2^p(x) = \frac{4}{9}\,x\left[u^p(x) + \bar{u}^p(x)\right] + \frac{1}{9}\,x\left[d^p(x) + \bar{d}^p(x)\right] + \frac{1}{9}\,x\left[s^p(x) + \bar{s}^p(x)\right] \qquad (2.9a)$$

$$\nu W_2^n(x) = \frac{4}{9}\,x\left[d^p(x) + \bar{d}^p(x)\right] + \frac{1}{9}\,x\left[u^p(x) + \bar{u}^p(x)\right] + \frac{1}{9}\,x\left[s^p(x) + \bar{s}^p(x)\right] \qquad (2.9b)$$

Data on the structure functions, together with neutrino nucleon scattering results that imply very little momentum carried by anti-quarks or strange quarks within the proton, leads to the quark distributions shown in Fig. 3a[15] ($u^p(x)$ = number of up quarks inside a proton with fractional momentum between

x and x + dx; $d^p(x)$ = number of down quarks ... etc.). The distributions $xu^p(x)$ and $xd^p(x)$ shown in Fig. 2a behave like $(1 - x)^3$ near x = 1 and $xu^p(x) = xd^p(x) = 0.15$ at x = 0. In addition the total fraction of momentum (area under curve) carried by charged quarks within the proton is 55%.

Unfortunately the pion structure function $\nu W_2^{\pi^+}(x)$ is not known and thus the behavior of the quark distributions within a pion are open to some speculation. The most naive use of dimensional counting plus the Drell-Yan relation between the inelastic structure function $\nu W_2(x)$ and the pion form factor yields $\nu W_2^{\pi^+}(x) \sim (1 - x)$ for $x \to 1$[16]. Feynman has pointed out that this result in fact neglects the fact that the pion has spin 0 and the quark has spin 1/2. This mismatch in the spins (which does not occur for the spin 1/2 proton) results in a pion structure function which behaves like $\nu W_2^{\pi^+}(x) \sim$ constant as $x \to 1$[17]. For completeness we consider both possibilities as shown in Fig. 3b and 3c[18]. In both cases the quark distributions are normalized so that the total fraction of momentum carried by the quarks is similar to that for the proton (about 50%). In addition the behavior at x = 0 is related via Regge behavior[19] (Pomeron exchange) to total cross sections by

$$xu^p(x)/xu^{\pi^+}(x) \xrightarrow[x\to 0]{} \sigma_{tot}(pp)/\sigma_{tot}(\pi p) \simeq 3/2. \qquad (2.10)$$

III. Results.

Figures 4 and 5 show the preliminary data on $R = \sigma(pp \to \pi^o X)/\sigma(\pi^+ p \to \pi^o X)$ versus $p_\perp$ at $\theta_{cm} = 90^o$ and $p_{lab} = 100$ and 200 GeV/c, respectively. At small $p_\perp$ the ratio is roughly given by $\sigma_{tot}(pp)/\sigma_{tot}(\pi^+ p) \simeq 1.5$. As $p_\perp$ increases the data at 100 and 200 GeV/c show somewhat different behavior. At 200 GeV/c the ratio R decreases slightly never falling much below one. At 100 GeV/c, on the other hand, R decreases more rapidly yielding a value $\simeq 0.4$ at $p_\perp = 3.0$ GeV/c.

The quark-quark scattering picture predicts that at fixed θ_{cm} the ratio R is a universal function of $x_\perp$ (or x_R) independent of p_{lab}. In fact power counting (Sec. II) yields $R \sim (1 - x_\perp)^3$ for $xu^{\pi^+}(x) \sim$ constant and $R \sim (1 - x_\perp)^2$ for $xu^{\pi^+}(x) \sim (1 - x)$. Fig. 6 shows the data for the two energies plotted versus $x_\perp$ compared with the universal curve predicted from the quark-quark scattering model (for the solid curve we took $xu^{\pi^+}(x) \sim 0.25$ as in Fig. 3b and the dashed curve represents $xu^{\pi^+}(x) \sim (1 - x)$ as in Fig. 3c). The data do behave qualitatively like the solid curve although there appears to be some scale breaking near $x_\perp = 0.2$[20]. It must be remembered that $x_\perp = 0.2$ at $p_{lab} = 100$ GeV/c corresponds to a $p_\perp$ value of only 1.3 GeV/c where there is undoubtedly some normal "hadronic background" (non-quark-quark scattering events).

This qualitative success of the simple quark-quark scattering approach is indeed intriguing and warrants further investigation. Particularly interesting quantities to investigate are the average values $\langle x_i \rangle$ of x's involved in the quark-quark scattering process shown in Fig. 2. Fig. 7 shows these mean values calculated from the quark-quark scattering model with $xu^{\pi^+}(x)$ as in Fig. 3b. Clearly at a given $p_\perp$ $\langle x_a \rangle$ is closer to one for $p_{lab} = 100$ GeV/c than 200 GeV/c (actually at fixed θ_{cm} $\langle x_a \rangle$ is a function of $x_\perp$ only). This results in the predicted R being different at a given $p_\perp$ for $p_{lab} = 100$ and 200 GeV/c. As we probe the beam closer to $\langle x_a \rangle$ equal to one we see more and more π^0's being produced by the π^+ relative to the proton beam due to the different quark distributions shown in Fig. 3d. Unfortunately even at $p_\perp = 3.0$ GeV/c and $p_{lab} = 100$ GeV/c the average value $\langle x_a \rangle$ is only about 1/2. We would of course like to probe the beam more thoroughly (closer to $\langle x_a \rangle = 1$). This can be accomplished by going to higher $p_\perp$ values or by going to a different θ_{cm} value. At $\theta_{cm} = 90^\circ$ $\langle x_a \rangle = \langle x_b \rangle$; however at $\theta_{cm} = 30^\circ$ $p_{lab} = 200$ GeV/c, for example, $\langle x_a \rangle$ is considerably greater than $\langle x_b \rangle$. At $p_\perp = 3.0$ GeV/c, $p_{lab} = 200$ GeV/c and $\theta_{cm} = 30^\circ$ Fig. 7 shows that $\langle x_a \rangle \simeq 0.8$! This results in the prediction that $R \simeq 0.04$ (see Fig. 8) at this $p_\perp$, p_{lab} and θ_{cm} value.

At any fixed θ_{cm} the quark-quark scattering model predicts that R is a function of only $x_\perp$ (or x_R). Fig. 9 shows the predictions at $\theta_{cm} = 90^o$ and 30^o together with the ranges covered for data taken with $0.5 \leq p_\perp \leq 4$ GeV/c and $p_{lab} = 200$ GeV/c, $\theta_{cm} = 90^o$ and 30^o; and $p_{lab} = 100$ GeV/c, $\theta_{cm} = 90^o$. Clearly data at $\theta_{cm} = 30^o$ is crucial in verifying the high x_R tail of the predicted R.

IV. Summary and Conclusions.

We make the following comments and conclusions:

1. The simple $q + q \to q + q$ scattering picture shown in Fig. 2a predicts that the ratio R is only a function of $x_\perp$ at fixed θ_{cm}. If instead the basic constituent scattering process is not $q + q \to q + q$ but something more complicated like, for example, $q + p \to q + B^*$ (and $q + \pi^+ \to q + \pi^*$) then $pp \to \pi^o X$ and $\pi^+ p \to \pi^o X$ would have different $p_\perp$ dependences (at fixed $x_\perp$, θ_{cm}).

2. The experimental values of R shown in Fig. 6 rule out the possibility that anti-quarks within the proton play an important role at these energies. Terms like $\bar{q}q \to \pi^o\pi^o$ result in many more π^o's being produced by the π^+ beam than by the proton beam (see Fig. 6). Anti-quarks carry a much greater fraction of the momentum in the π^+ than in the proton (see the distributions in Fig. 3).

3. In the $q + q \to q + q$ scattering picture the value of $R \approx 1.5$ seen at small $x_\perp$ (Fig. 6) is a natural consequence of (2.10). The pion and proton structure functions are assumed to have Regge behavior[19] near $x = 0$ and are related at $x = 0$ by $\sigma_{tot}(pp)/\sigma_{tot}(\pi^+ p) \approx 1.5$. Once other terms with different structure functions are allowed this behavior might not be as natural.

4. It must be remembered that we did not perform any fitting to the data in this paper. The predictions made are natural consequences of a $q + q \to q + q$ scattering picture. The pion structure function and/or

the modifications of $d\hat{\sigma}/d\hat{t}$ could be varied slightly to make agreement with the data perfect.

5. Independent of whether or not the simple quark-quark scattering picture is correct the kinematics shown in Fig. 7 indicate that it is crucial to measure R at smaller θ_{cm} values in order to probe the beam closer to $\langle x_a \rangle = 1$.

Acknowledgements.

We are indebted to R. P. Feynman for many useful and stimulating discussions. In fact Feynman performed estimates of R based on a simple quark-quark scattering picture which agreed with the "super-preliminary" data.

References and Footnotes

1. J. D. Bjorken and E. A. Paschos, Phys. Rev. 185, 1975 (1967).
2. R. P. Feynman, Phys. Rev. Letters 23, 1415 (1969); and R. P. Feynman, Photon-Hadron Interactions, (W. A. Benjamin, Reading, Mass., 1972).
3. S. M. Berman, J. D. Bjorken, and J. Kogut, Phys. Rev. D4, 3388 (1971); J. D. Bjorken, Phys. Rev. D8, 4078 (1973).
4. For a review of the various models including the hard-scattering approach see, D. Sivers, S. J. Brodsky, and R. Blankenbecler, "Large Transverse Momentum Processes," SLAC-PUB-1595 (1975), to be published in Physics Reports.
5. See, for example, R. Blankenbecler, S. J. Brodsky and J. Gunion, SLAC-PUB-1585 (1975), to be published in Phys. Rev.
6. Also see, S. D. Ellis and M. B. Kislinger, Phys. Rev. D9, 2027 (1974).
7. R. Blankenbecler, S. J. Brodsky, and J. F. Gunion, Phys. Rev. 106, 2652 (1972); Phys. Letters 42B, 461 (1973); R. Blankenbecler, S. J. Brodsky, Phys. Rev. D10, 2973 (1974); J. F. Gunion, Phys. Rev. D10, 242 (1974).
8. D. Amati, L. Caneschi, and M. Testa, Phys. Letters, 48B, 186 (1973).
9. In deriving (2.1) and (2.2) we have assumed all masses are negligible.
10. The ISR data show a $1/p_\perp^8$ dependence at fixed $x_\perp$ and $\theta = 90^\circ$, while the FNAL data yield a $p_\perp$ dependence closer to $1/p_\perp^{12}$.
11. This is the direction chosen by the CIM people (Ref. 5 and 7).
12. S. D. Ellis, Phys. Letters 49B, 189 (1974).
13. See, for example, R. F. Cahalan, K. A. Geer, J. Kogut, and L. Susskind, Cornell preprint CLNS-289 (1974); H. M. Friend and T. K. Gasiser, Phys. Rev. D7, 741 (1973), D4, 3330 (1971), D6, 2560 (1972). None of the above approaches is successful at fitting the existing data but they indicate possible ways of modifying the basic quark-quark interaction.

14. This is done by simply multiplying the $d\hat{\sigma}/d\hat{t}(\hat{s},\hat{t};\ qq \to qq)$ given in (2.8) by $1/\hat{s}^4$.

15. Glennys R. Farrar, Nucl. Phys. B77, 429 (1974).

16. This is the behavior assumed by the CIM people of Ref. 5 and 7.

17. R. P. Feynman (private communication). Although not stated explicity, this behavior for $\nu W_2^{\pi^+}(x)$ is clear from the discussions in Feynman's book, Photon-Hadron Interactions (Ref. 2).

18. The distribution $H_{q\to\pi}(x_c)$ for a quark materializing into a cloud of hadrons containing one π^o with momentum fraction x_c is in general not equal to the reverse distribution $G_{\pi\to q}(x)$. We assume, however, that the behavior near "threshold", $x_c = 1$, of the probability that a quark is one hard hadron (+wee hadrons) is very similar to the behavior of the probability that the same hadron is one hard quark (+wee quarks). In fact, since the calculations are sensitive to $H_{q\to\pi}(x_c)$ only near $x_c = 1$ (see mean values in Fig. 7), we assume for simplicity that $H_{q\to\pi}(x) = G_{\pi\to q}(x)$. In principle H(x) can be measured in the leptonic process $\ell p \to \ell + \pi + X$, where the π is in the so-called current fragmentation region or by measuring the process $e^+e^- \to \pi + X$. Data, however, exist only for $x_c \leq 0.8$ and as mentioned above the calculations are sensitive to $x_c \geq 0.9$.

19. In deep inelastic electron scattering the structure function $\nu W_2(Q^2,\nu)$ is related to the total cross section for virtual photon (γ_v) proton scattering where ν is the photon energy and Q^2 is the photon "mass". This cross section is related via the optical theorem to the imaginary part of the virtual photon proton elastic amplitude. In the scaling region where $\nu W_2(x)$ is a function of only $x = Q^2/2m\nu$, the limit $x \to 0$ implies keeping Q^2 fixed and increasing the energy ν, which is just the Regge region for the virtual photon proton elastic scattering amplitude. Assuming Pomeron exchange yields $\sigma_{tot}(\gamma_v p)/\sigma_{tot}(\gamma_v \pi^+) = \sigma_{tot}(pp)/\sigma_{tot}(\pi^+ p) \simeq 3/2$.

20. Some scale breaking is expected even from the quark-quark scattering model. This is due to the fact that the structure functions $\nu W_2(Q^2,\nu)$ and hence the quark distributions (2.9) are in general functions of both Q^2 and ν. Only when Q^2 and ν are large does one expect scaling (i.e. $\nu W_2(x)$). Perhaps the quark distributions have a slight dependence on the proton momentum (i.e. p_{lab}) and that the small scale breaking seen in the data will dissappear with increasing energy.

Figure Captions

Fig. 1: Illustration of the common underlying structure of constituent or "hard-scattering" models. The large transverse momentum reaction A + B → C + X is assumed to occur as a result of a single large angle scattering a + b → c + d of constituents a and b, followed in general by the decay or fragmentation of c into the observed particle C.

Fig. 2:

(a) Illustration of the quark-quark scattering model for $p(\pi^+) + p \to \pi^o + X$, where $u^{p,\pi^+}(x_a)$ is the probability for the quark q (up quark) to have fractional longitudinal momentum x_a of the beam (proton or π^+).

(b) Illustration of the gluon exchange mechanism for producing large angle qq → qq scattering $d\hat{\sigma}/d\hat{t}(\hat{s},\hat{t})$.

Fig. 3:

(a) The quark distributions $xu^p(x)$, $xd^p(x)$ and the anti-quark distribution $x\bar{u}^p(x)$ within a proton, where u = up quarks, d = down quarks, and $\bar{u}$ = anti-quarks (taken from Ref. 15).

(b) The quark distributions $xu^{\pi^+}(x) = x\bar{d}^{\pi^+}(x)$ within a π^+, where it is assumed that $\nu W_2^{\pi^+}(x) \sim 0.25$ for $x \to 1$.

(c) Same as (b) but $\nu W_2^{\pi^+}(x) \sim (1 - x)$ for $x \to 1$ (taken from Ref. 15).

(d) Comparison of the quark distributions for a proton $(xu^p(x) + xd^p(x))/2$ and a $\pi^+ (xu^{\pi^+}(x) = x\bar{d}^{\pi^+}(x))$.

Fig. 4: The ratio R of the 100 GeV/c invariant cross sections at 90^o for $pp \to \pi^o X$ and $\pi^+ p \to \pi^o X$, plotted as a function of $p_\perp$. The data are preliminary results from Fermilab Experiment #268 (BNL/LBL/CIT collaboration).

Fig. 5: The ratio R of the 200 GeV/c invariant cross sections at 90^{o} for $pp \to \pi^{o}X$ and $\pi^{+}p \to \pi^{o}X$, plotted as a function of $p_{\perp}$. The data are preliminary results from Fermilab Experiment #268 (BNL/LBL/CIT collaboration).

Fig. 6: Shows the ratio $R = \sigma(pp \to \pi^{o}X)/\sigma(\pi^{+}p \to \pi^{o}X)$ at $\theta_{cm} = 90^{o}$ plotted versus $x_{\perp}$, together with the predictions of the quark-quark scattering model (Fig. 2a), where the π^{+} structure function is assumed to behave like $\nu W_2^{\pi}(x) \sim 0.25$ (Fig. 3b, solid curve) and like $\nu W_2^{\pi^{+}}(x) \sim (1 - x)$ (Fig. 3c, dashed curve). These models predict that R is a function of only $x_{\perp}$ at fixed θ_{cm}. Also shown (dotted curve) is the predicted R for anti-quark-quark scattering, where the proton anti-quark distribution is shown in Fig. 3a and $x\bar{d}^{\pi^{+}}(x) \sim 0.25$ as in Fig. 3b.

Fig. 7:

(a) Shows the mean value $\langle x_a \rangle$ of the proton and π^{+} beam at $\theta_{cm} = 90^{o}$, $p_{lab} = 100$ GeV/c versus $p_{\perp}$. Note that at $\theta_{cm} = 90^{o}$ $\langle x_a \rangle \simeq \langle x_b \rangle$. The error bars correspond to the calculated root-mean-square deviations of x_a.

(b) Similar to (a) but for $p_{lab} = 200$ GeV/c.

(c) Similar to (a) but for $p_{lab} = 200$ GeV/c and $\theta_{cm} = 30^{o}$. Notice that $\langle x_a \rangle_{beam}$ no longer equals $\langle x_b \rangle_{target}$ and that for a given $p_{\perp}$ one is probing $\langle x_a \rangle$ closer to one than at 90^{o}.

(d) Shows the mean value $\langle x_c \rangle = \langle p_{\pi o}/p_{quark} \rangle$ of the observed π^{o} at 100 GeV/c, $\theta_{cm} = 90^{o}$ versus $p_{\perp}$. In contrast to $\langle x_a \rangle$ this quantity is very close to one. At $p_{\perp} = 2.0$ GeV/c the observed π^{o} is carrying 90% of the momentum of the quark from which it came.

Fig. 8: Predictions for the ratio $R = \sigma(pp \to \pi^{o}X)/\sigma(\pi^{+}p \to \pi^{o}X)$ versus $p_{\perp}$ from the quark-quark scattering model shown in Fig. 2a and

where we have assumed $\nu W_2^{\pi}(x) \sim 0.25$ as shown in Fig. 3b. Notice the rapid variation of R with center of mass scattering angle θ_{cm}.

Fig. 9: Shows the predicted values for $R = \sigma(pp \to \pi^o X)/\sigma(\pi^+ p \to \pi^o X)$ at $\theta_{cm} = 90^o$ and $\theta_{cm} = 30^o$ versus x_R ($x_R^2 = x_\perp^2 + x_{||}^2$) from the quark-quark scattering model shown in Fig. 2a and where we have assumed $\nu W_2^{\pi^+}(x) \sim 0.25$ as shown in Fig. 3b. The model predicts that R is a function of only x_R at fixed θ_{cm}. Also shown are the kinematic ranges covered by experiments with $0.5 \leq p \leq 4.0$ GeV/c and (i) $p_{lab} = 100$ GeV/c, $\theta_{cm} = 90^o$; (ii) $p_{lab} = 200$ GeV/c, $\theta_{cm} = 90^o$; (iii) $p_{lab} = 200$ GeV/c, $\theta_{cm} = 30^o$.

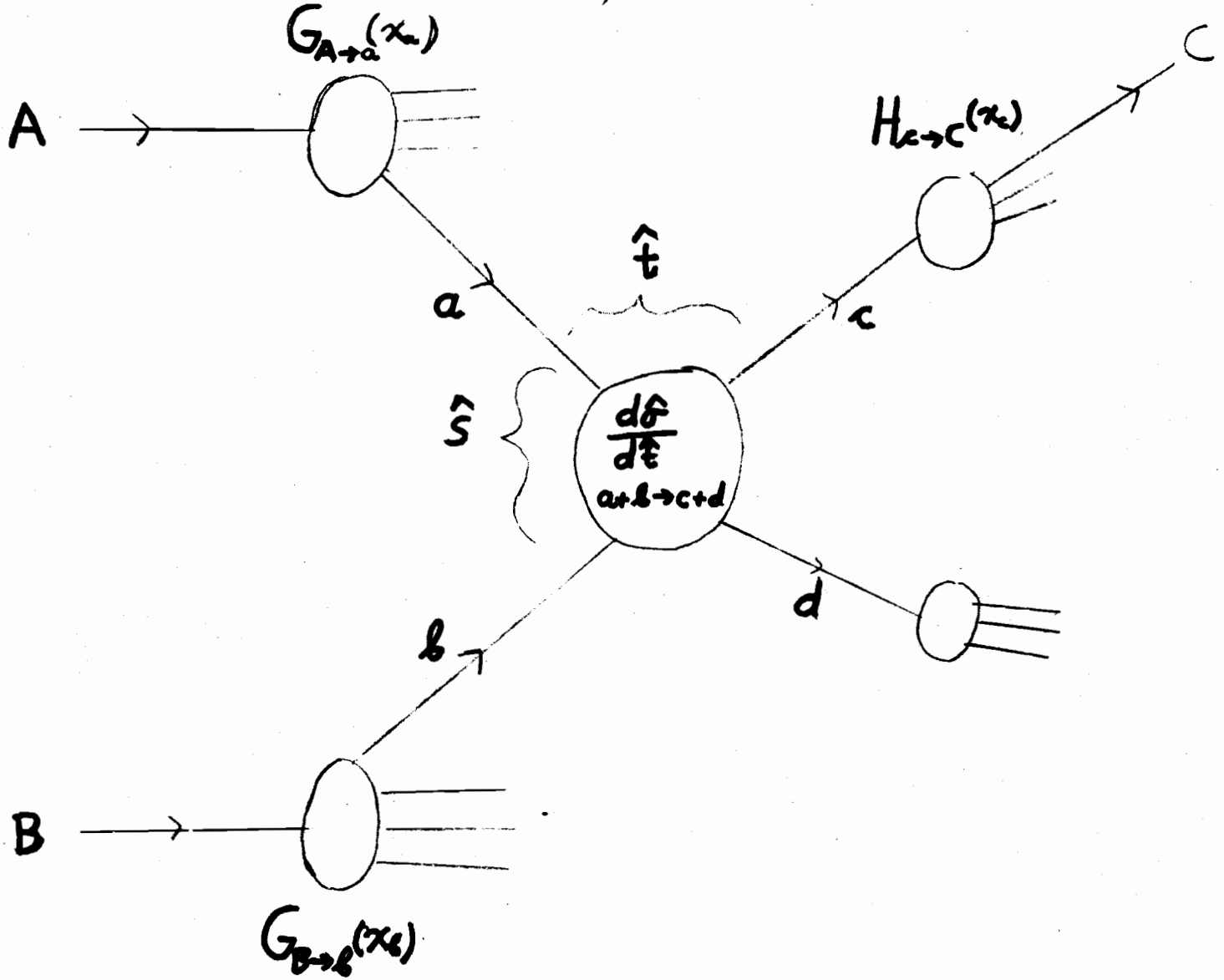
$G_{A\to a}(x_a)$
A
C
$H_{c\to C}(x_c)$
$\hat{t}$
a
c
$\hat{s}$
$\frac{d\hat{\sigma}}{d\hat{t}}$
$a+b\to c+d$
d
b
B
$G_{B\to b}(x_b)$

Fig. 1 $A+B\to C+X$

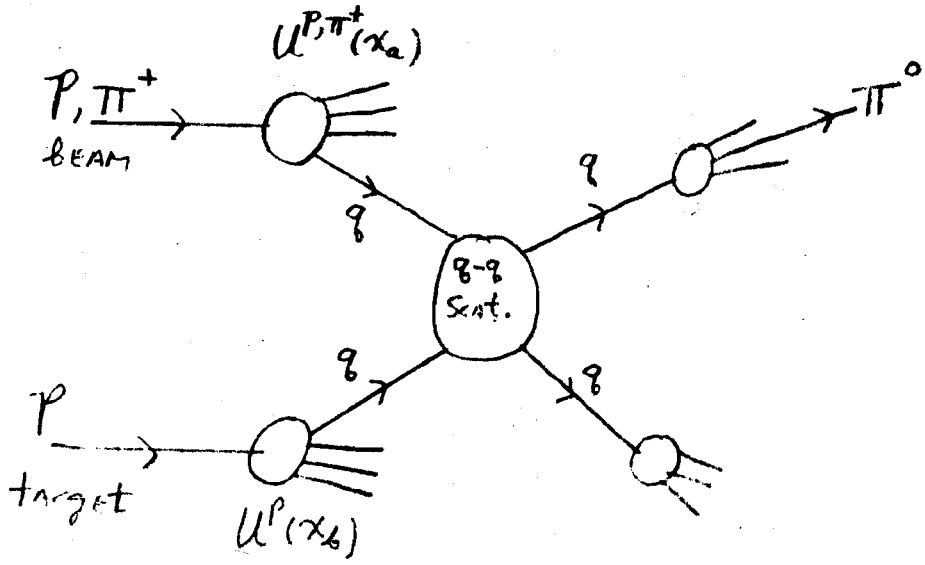
$U^{p,\pi^+}(x_a)$
p, π^+
BEAM
π^0
q
q
q-q
Scat.
q
q
p
target
$U^p(x_b)$

Fig. 2a

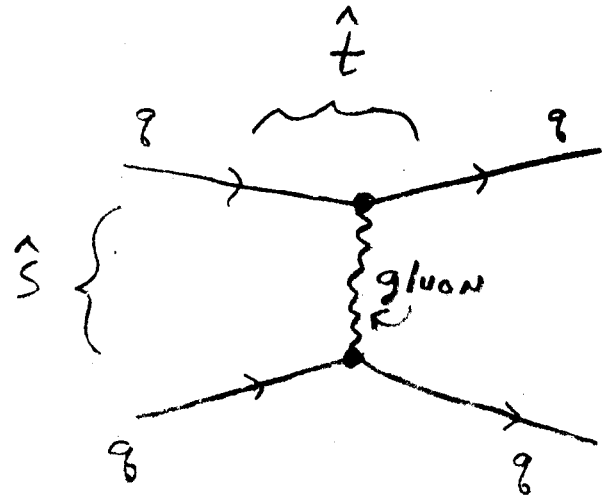
$\hat{t}$
q
q
$\hat{s}$
gluon
q
q

Fig. 2b

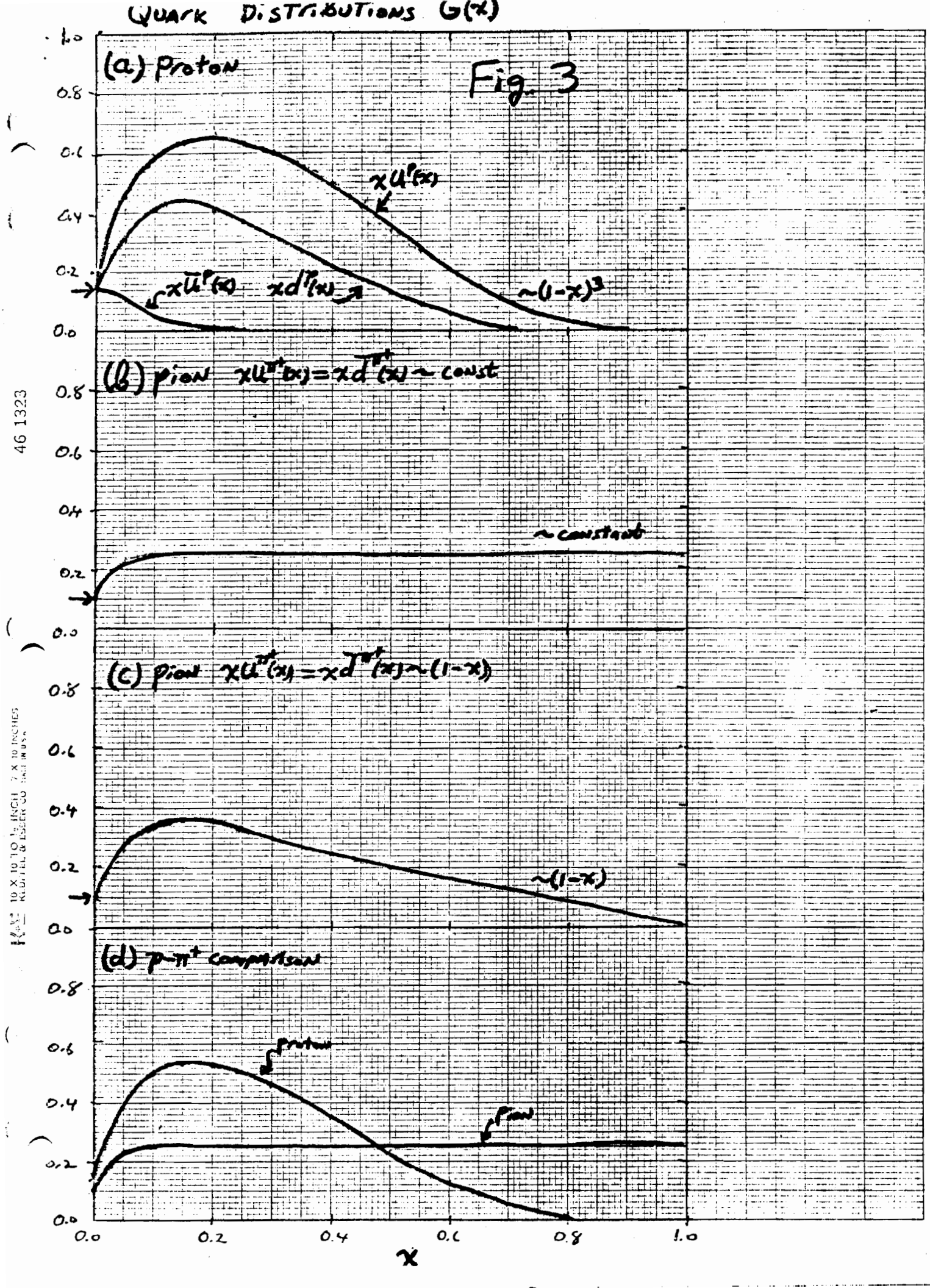
QUARK DISTRIBUTIONS G(x)
Fig. 3
(a) Proton
$xu^p(x)$
$xd^p(x)$
$\sim(1-x)^3$
(b) pion $xu^{\pi^+}(x) = xd^{\pi^+}(x) \sim$ const
$\sim$ constant
(c) pion $xu^{\pi^+}(x) = xd^{\pi^+}(x) \sim (1-x)$
$\sim(1-x)$
(d) p-π^+ comparison
proton
pion
1.0
0.8
0.6
0.4
0.2
0.0
0.0
0.2
0.4
0.6
0.8
1.0
x

Fig. 4

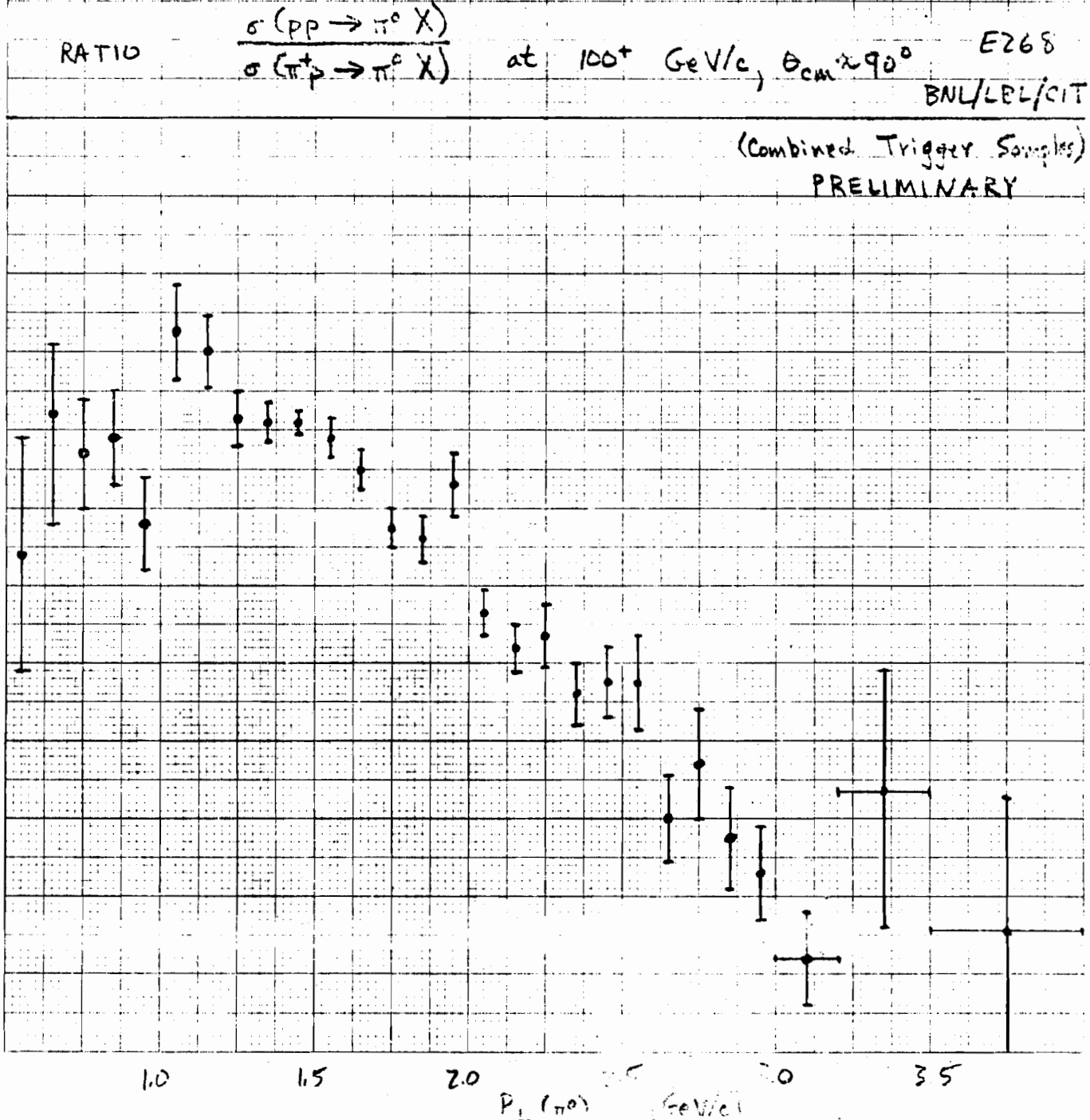

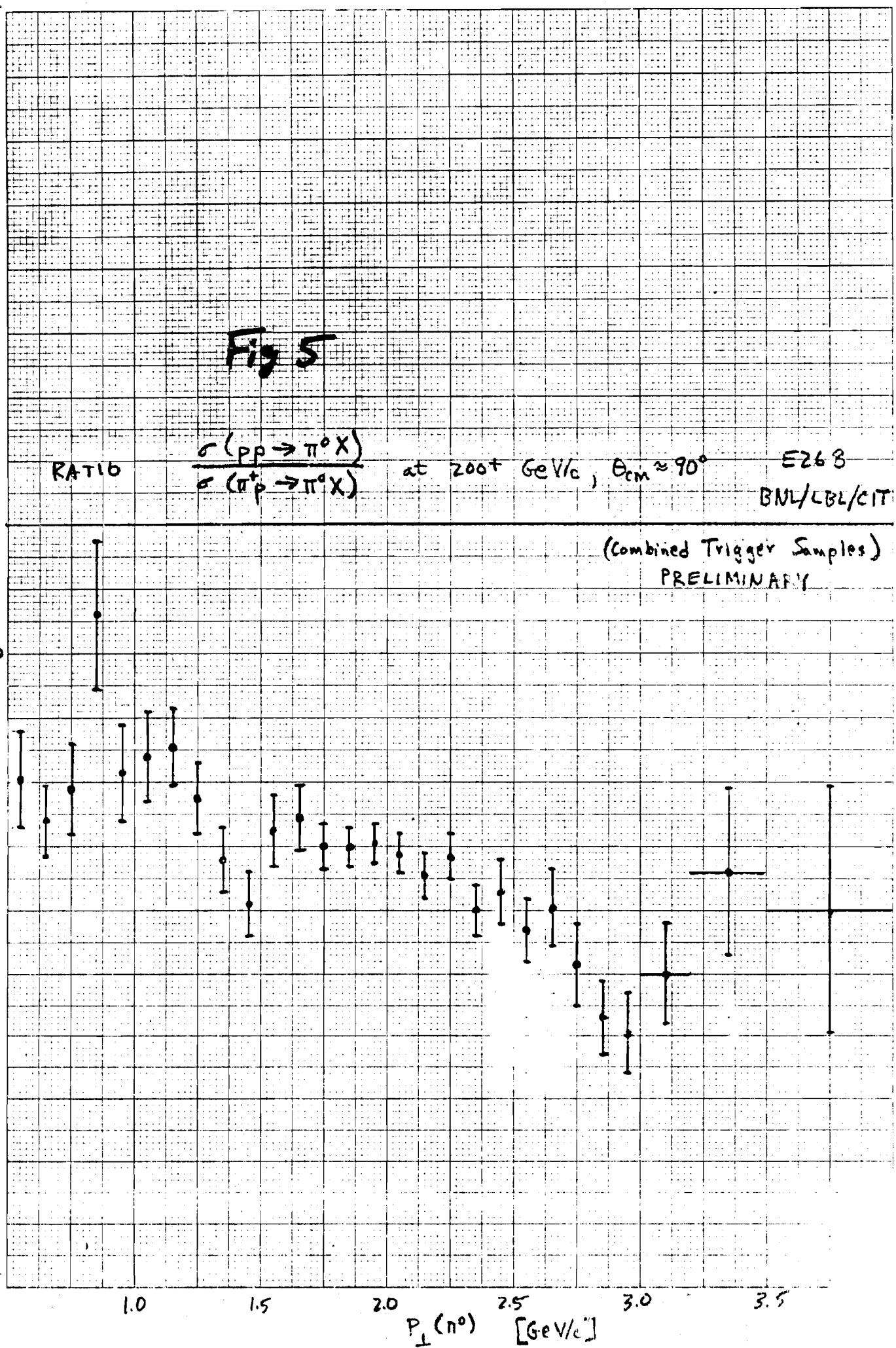

RATIO $\frac{\sigma(pp \to \pi^0 X)}{\sigma(\pi^+ p \to \pi^0 X)}$ at $\theta_{cm} \approx 90°$ versus $X_\perp = \frac{2P_\perp}{\sqrt{s}}$

E268
BNL/LBL/CIT

Fig. 6

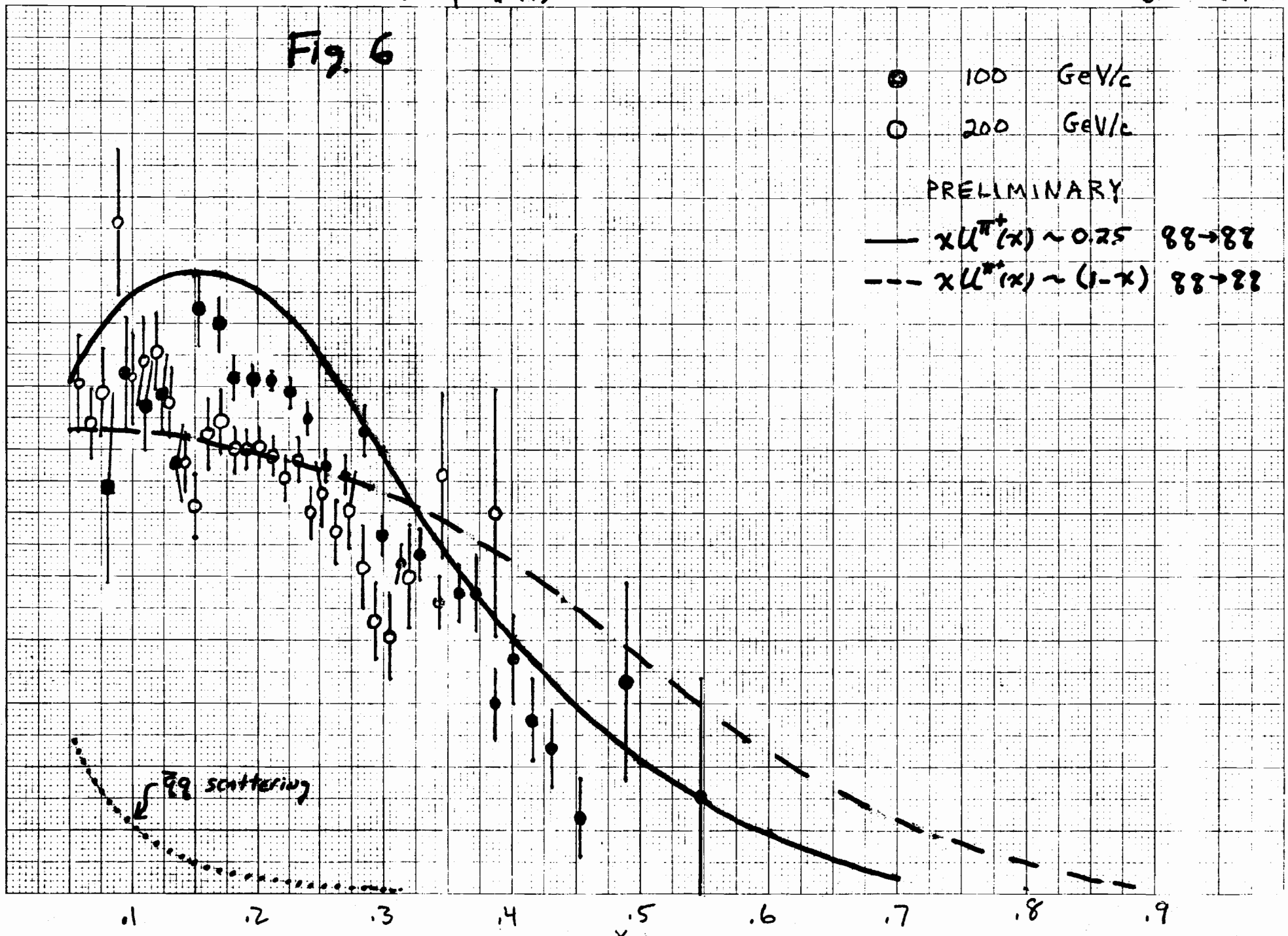

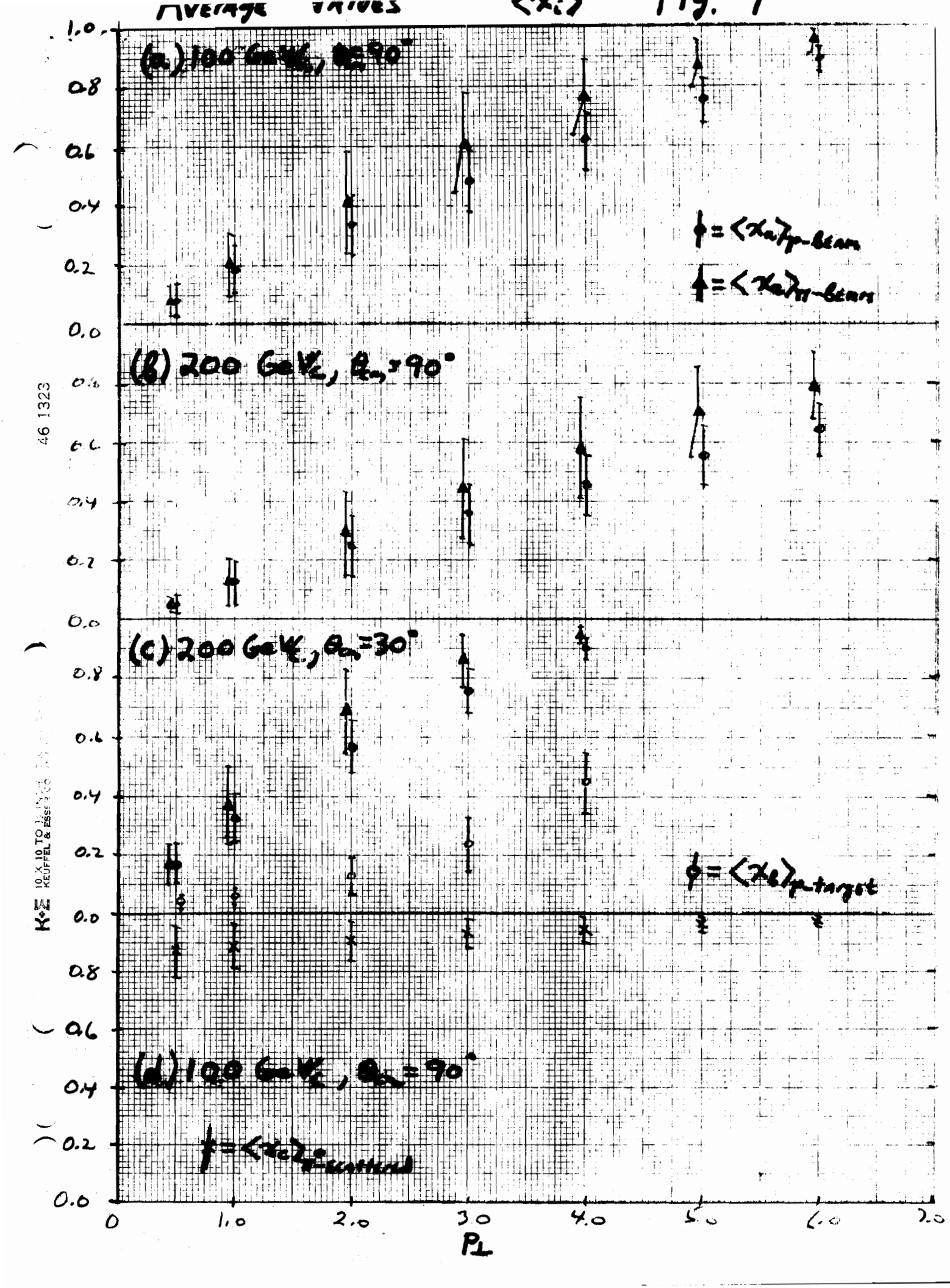
Average values $\langle x_i \rangle$ Fig. 1
(a) 100 GeV/c, θ_{cm}=90°
$\phi = \langle x_a \rangle_{p\text{-beam}}$
$\phi = \langle x_a \rangle_{\pi\text{-beam}}$
(b) 200 GeV/c, θ_{cm}=90°
(c) 200 GeV/c, θ_{cm}=30°
$\phi = \langle x_b \rangle_{p\text{-target}}$
(d) 100 GeV/c, θ_{cm}=90°
$\phi = \langle x_c \rangle_{\pi^0\text{-scattered}}$
1.0
0.8
0.6
0.4
0.2
0.0
0
1.0
2.0
3.0
4.0
5.0
6.0
7.0
P_L
46 1323
10 X 10 TO 1 INCH
KEUFFEL & ESSER CO.

$R = \sigma(pp \to \pi^0 X) / \sigma(\pi p \to \pi^0 X)$ vs. $P_\perp$ Fig 8

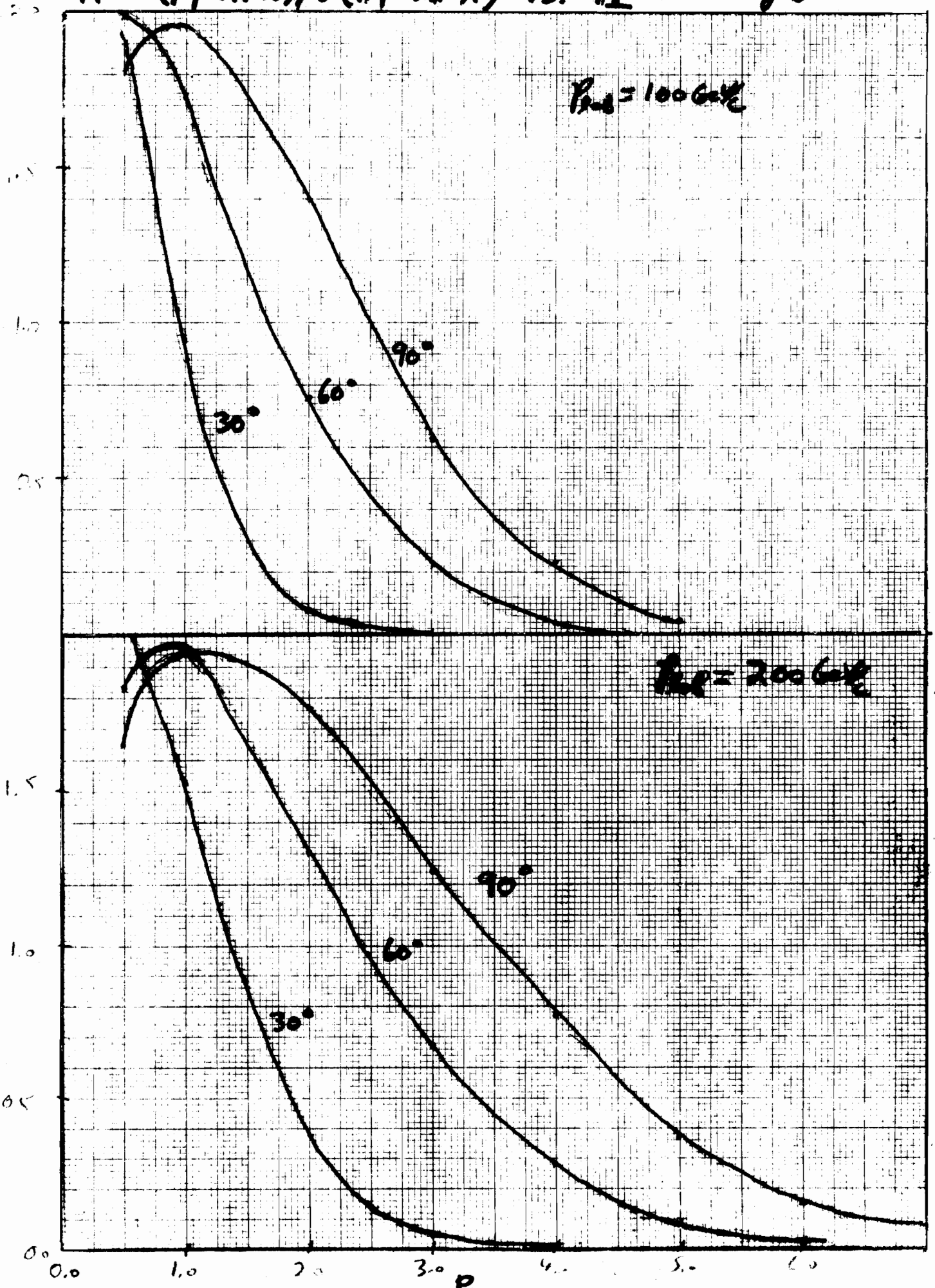

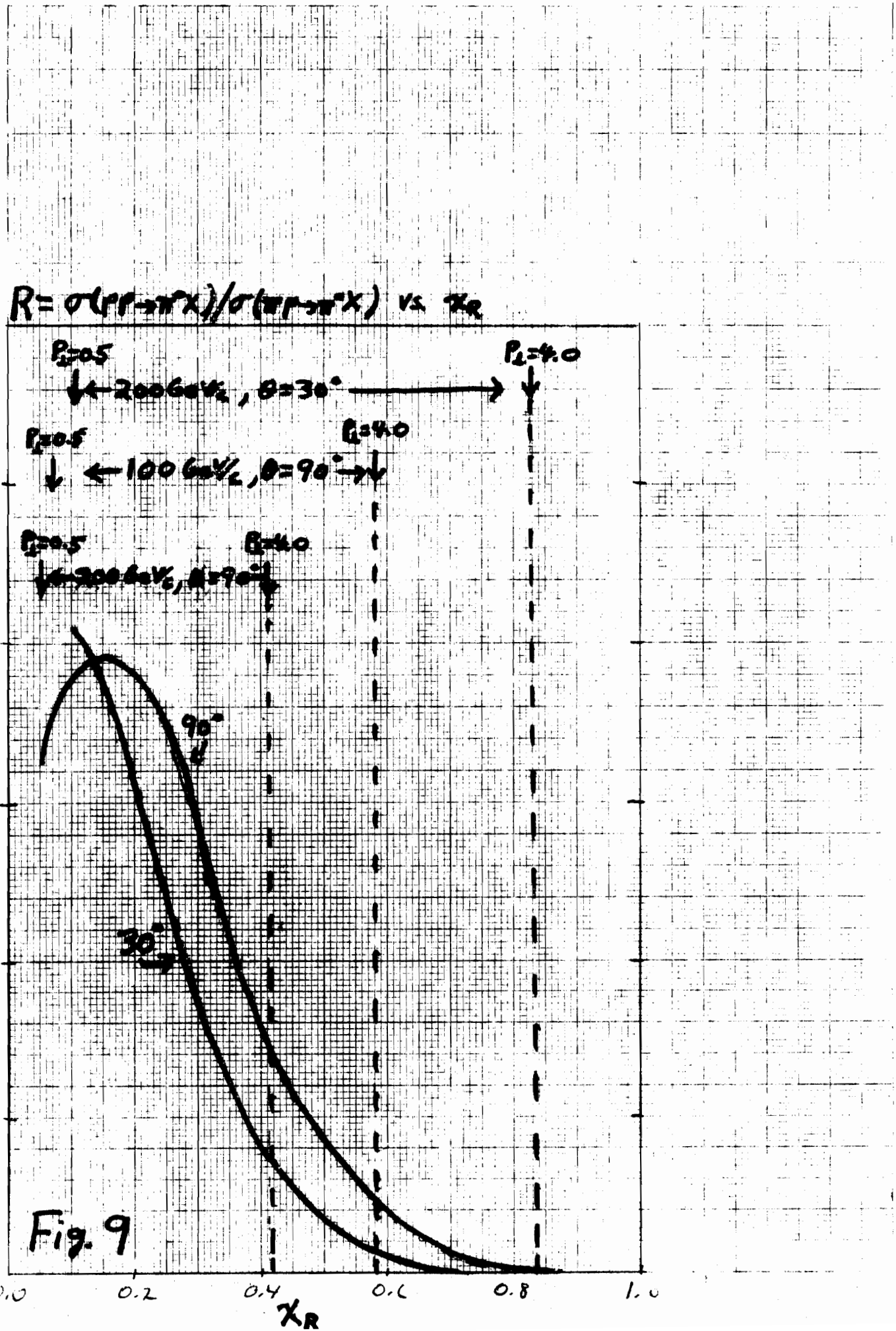
R = σ(pp→π⁺X)/σ(π⁻p→π⁻X) vs. χR
P⊥=0.5
←2.0 GeV/c, θ=30°→
P⊥=4.0
P⊥=0.5
←1.0 GeV/c, θ=90°→
P⊥=4.0
P⊥=0.5
←2.0 GeV/c, θ=90°→
P⊥=4.0
90°
30°
3.0
2.5
2.0
1.5
1.0
0.5
0.0
0.0
0.2
0.4
0.6
0.8
1.0
χR

Fig. 9